Title

Marine latitude/altitude OH distributions: Comparison of Pacific Ocean observations with models

Journal

Journal of Geophysical Research Atmospheres, 106(D23)

ISSN

0148-0227

Authors

Davis, D
Grodzinsky, G
Chen, G
et al.

Publication Date

2001-12-16

DOI

10.1029/2001JD900141

JOURNAL OF GEOPHYSICAL RESEARCH, VOL. 106, NO. D23, PAGES 32,691–32,707, DECEMBER 16, 2001

Marine latitude/altitude OH distributions: Comparison of Pacific Ocean observations with models

D. Davis,[1] G. Grodzinsky,[1] G. Chen,[1] J. Crawford,[2] F. Eisele,[1,3] L. Mauldin,[3] D. Tanner,[1] C. Cantrell,[3] W. Brune,[4] D. Tan,[4] I. Faloona,[4] B. Ridley,[3] D. Montzka,[3] J. Walega,[3] F. Grahek,[3] S. Sandholm,[1] G. Sachse,[2] S. Vay,[2] B. Anderson,[2] M. Avery,[2] B. Heikes,[5] J. Snow,[5] D. O'Sullivan,[6] R. Shetter,[3] B. Lefer,[3] D. Blake,[7] N. Blake,[7,8] M. Carroll,[9] and Y. Wang[1,10]

Abstract. Reported here are tropical/subtropical Pacific basin OH observational data presented in a latitude/altitude geographical grid. They cover two seasons of the year (spring and fall) that reflect the timing of NASA's PEM-Tropics A (1996) and B (1999) field programs. Two different OH sensors were used to collect these data, and each instrument was mounted on a different aircraft platform (i.e., NASA's P-3B and DC-8). Collectively, these chemical snapshots of the central Pacific have revealed several interesting trends. Only modest decreases (factors of 2 to 3) were found in the levels of OH with increasing altitude (0-12 km). Similarly, only modest variations were found (factors of 1.5 to 3.5) when the data were examined as a function of latitude (30°N to 30°S). Using simultaneously recorded data for CO, O_3, H_2O, NO, and NMHCs, comparisons with current models were also carried out. For three out of four data subsets, the results revealed a high level of correspondence. On average, the box model results agreed with the observations within a factor of 1.5. The comparison with the three-dimensional model results was found to be only slightly worse. Overall, these results suggest that current model mechanisms capture the major photochemical processes controlling OH quite well and thus provide a reasonably good representation of OH levels for tropical marine environments. They also indicate that the two OH sensors employed during the PEM-Tropics B study generally saw similar OH levels when sampling a similar tropical marine environment. However, a modest altitude bias appears to exist between these instruments. More rigorous instrument intercomparison activity would therefore seem to be justified. Further comparisons of model predictions with observations are also recommended for nontropical marine environments as well as those involving highly elevated levels of reactive non-methane hydrocarbons.

1. Introduction

Since the early 1970s when free radicals were first recognized as critical chemical components of the atmosphere, a major effort has been underway to establish a quantitative understanding of these species and their chemistry [*Levy*, 1971, 1972]. Two of the most important of these radicals are the hydroxyl, OH, and hydroperoxy, HO_2, species. As the most important tropospheric oxidant, OH provides the main atmospheric sink for most trace gases, thereby preventing their build up to toxic levels. The hydroperoxy radical, on the other hand, defines one of the most important pathways for converting NO to NO_2, and therefore is pivotal to our understanding of photochemically generated O_3.

A critical examination of the chemical processes driven by OH and HO_2 has only recently become possible with the development of new experimental techniques for making direct measurements of these species [*Eisele and Tanner*, 1991, 1993; *Mount*, 1992; *Tanner and Eisele*, 1995; *Wennberg et al.*, 1994, 1995; *Harder et al.*, 1997; *Brune et al.*, 1998]. Thus, early attempts to present global distributions of these species were limited to model projections [e.g., *Logan et al.*, 1981; *Chameides and Tan*, 1981; *Spivakovsky et al.*, 1990; *Hough*, 1991]. The lack of HO_x radical measuring capability has also had repercussions as related to testing our current understanding of fast photochemical processes. Most of the early testing was limited to the more measurement friendly species NO and NO_2, and the peroxides H_2O_2 and CH_3OOH [e.g., *Trainer et al.*, 1987; *Chameides et al.*, 1990; *Davis et al.*, 1993, 1996; *Fan et al.*,

[1]School of Earth and Atmospheric Sciences, Georgia Institute of Technology, Atlanta, Georgia, USA.
[2]NASA Langley Research Center, Hampton, Virginia, USA.
[3]National Center for Atmospheric Research, Boulder, Colorado, USA.
[4]Department of Meteorology, Pennsylvania State University, University Park, Pennsylvania, USA.
[5]Graduate School of Oceanography, University of Rhode Island, Narragansett, Rhode Island, USA.
[6]Department of Chemistry, United States Naval Academy, Annapolis, Maryland, USA.
[7]Department of Chemistry, University of California-Irvine, Irvine, California, USA.
[8]Institute of the Study of Earth, Ocean and Space, University of New Hampshire, Durham, New Hampshire, USA.
[9]Department of Atmospheric, Oceanic and Space Sciences, University of Michigan, Ann Arbor, Michigan, USA.
[10]Department of Environmental Sciences, Rutgers University, New Brunswick, New Jersey, USA.

Paper number 2001JD900141.
0148-0227/01/2001JD900141$09.00

1994; *Crawford et al.*, 1996; *Heikes*, 1992; *Heikes et al.*, 1996a, 1996b; *Penkett et al.*, 1998; *Ayers et al.*, 1992, 1996; *Schultz et al.*, 1998; *Bradshaw et al.*, 1998; *Hauglustaine et al.*, 1999]. With the arrival of new techniques for measuring HO_x radicals, this testing has now taken on a more definitive character. Hydroxyl and hydroperoxy radical observations define two of the most sensitive test points for evaluating these mechanisms [e.g., *Wennberg et al.*, 1998; *Jaeglé et al.*, 1998, 1999; *McKeen et al.*, 1997; *Brune et al.*, 1999; *Eisele et al.*, 1996; *Mauldin et al.*, 1998; *Jefferson et al.*, 1998; *Wang and Jacob*, 1998; *Crawford et al.*, 1999a; *Chen et al.*, 2001, and references therein]. Tests involving these species have been limited to date, but already have begun to provide some idea of the range of disagreement that can be found between box model predictions and observations. This has ranged from near perfect agreement to factors of 2 to 3. The typical 2σ uncertainty expressed in the observations (±45%) and that for box models (±60%) would lead one to think that the level of agreement should be within a factor of 2 to 2.5. However, this still assumes the mechanism being used in the model is basically correct, i.e., that only the values assigned to rate coefficients and other chemical input parameters provide a basis for disagreement. If, however, a yet unknown but significant chemical process is being totally left out of our current mechanisms, the above scenario is not true. Under these circumstances it becomes possible for much larger disagreements than factors of 2 to 2.5 to be realized.

In this paper we address the above issue as related to OH by taking advantage of the extensive data collected during NASA's PEM-Tropics A (1996) and B (1999) field programs. The region being addressed, the tropical Pacific, defines the single largest atmospheric zone responsible for the oxidation of tropospheric trace gases. Previously, there has been a heavy reliance on three-dimensional (3-D) models as the principal means for estimating the lifetimes for many of these gases. The current effort, directed toward developing a tropical geographical OH grid map using observational OH data, thus provides another check on the credibility of these earlier OH model projections.

It is noted that several parallel photochemical modeling efforts to this study have also used the PEM-Tropics B data base [*Olson et al.*, this issue; *Tan et al.*, this issue; *Mauldin et al.*, this issue, *Wang et al.*, this issue and *Ravetta et al.*, this issue]. In nearly all of these parallel efforts, however, model related comparison activity has involved the use of "point to point" observation/model comparisons. The current study analyzes the OH observational data only after assembling it into a geographical altitude/latitude grid map.

Since this study has drawn on OH data generated from two different measurement methods, we have also attempted to make a semiquantitative comparison between these two instruments. This comparison has again made use of the geographical altitude/latitude generated OH grid map. A totally independent assessment of the two aircraft OH sensors has been provided by *Eisele et al.* [this issue]. More in-depth analyses of OH and HO_2 chemical controlling processes have been presented in companion papers by *Wang et al.* [this issue]; *Tan et al.* [this issue]; *Ravetta et al.* [this issue].

2. Measurement Techniques

As previously noted, two different OH sensors were used to record the OH data used in this analysis. The first instrument, a selected ion chemical ionization mass spectrometer (SICIMS), was mounted on the NASA P-3B aircraft and reported OH data both during PEM-Tropics A and B. The SICIMS technique is an indirect measurement method for OH in that it does not measure the OH species itself, but rather, a stable ion that can be directly linked to OH through an added isotopically labeled reactant. Calibration of this system is achieved using ambient air by photolyzing H_2O at a known velocity with a photon flux of 184.9 nm radiation. The limit-of-detection (LOD) of the SICIMS system at both low and high altitudes is typically given as $2x10^5$ molecules cm^{-3}. The 2σ uncertainty in these measurements is cited as the combined error defined by the precision plus bias error, e.g., ± 40%. Further details concerning the SICIMS technique can be found in *Eisele and Tanner* [1991] and *Tanner and Eisele* [1995].

The second OH instrument labeled Airborne Tropospheric Hydrogen Oxide Sensor (ATHOS) was flown on the DC-8. It was available during PEM-Tropics B only. This laser-induced fluorescence sensor does make a direct measurement of OH. The instrument used during PEM-Tropics B was an updated version of the instrument flown earlier on NASA's SUCCESS and SONEX field studies. The in-flight "relative" calibration of the ATHOS system is similar to that used by the SICIMS instrument in that it involves the 184.9 nm photolysis of ambient H_2O/air mixtures. The LOD for ATHOS at low altitudes is given as $4x10^5$ molecules cm^{-3}, with upper tropospheric detection levels dropping to $1x10^5$ molecules cm^{-3}. The 2σ total error in the ATHOS measurement, again a combination of precision and bias error, is ± 50%. Further details concerning the ATHOS OH system can be found in *Brune et al.* [1998]. (Note, via the chemical titration of HO_2 with NO, the ATHOS system can also measure HO_2. These observations were not used in the current analysis; see instead, *Tan et al.* [this issue], *Olson et al.* [this issue], and *Ravetta et al.* [this issue]).

Other measurements recorded during PEM-Tropics A and B in support of the model simulations included: CO, O_3, NO, H_2O, NMHCs, ambient temperature, and pressure, and the UV irradiance or spectroradiometric readings. Additionally, some model sensitivity studies used observed values for H_2O_2 and CH_3OOH.

With the exception of the P-3B NO and NO_2 measurements, the same basic techniques and personnel used during PEM-Tropics A to measure chemical species and parameters were also employed during PEM-Tropics B. A description of these techniques and a listing of personnel involved have been provided in Overview Papers by *Hoell et al.* [1999] and *Raper et al.* [this issue]. Also provided in these papers are the detection limits and precision for all measurement techniques.

3. Model Descriptions and Approach

Both box model and 3-D model results were generated for comparison with the OH observational data. Details concerning each of these models is given below.

3.1. Box Model

Box model OH values were generated in this study using a time-dependent (TD) model similar to that previously described for other PEM related work [*Davis et al.*, 1996; *Crawford et al.*, 1997a, 1997b, 1999a; *Chen et al.*, 2001]. This model assumes that quasi-steady state levels are reached for all species. This means that upon reaching this state all species' diurnal profiles repeat themselves. Thus, although varying in time, they vary in a

predictable fashion. The model can be initialized once positive values are assigned to all input species for any point in time. The model mechanism is based on rate coefficients reported in the recommendations given by *DeMore et al.* [1997], and *Atkinson et al.* [1992]. Those of *DeMore et al.* [1997] were recently updated based on information provided at the web site http://jpldataeval.jpl.gov/DownLoad_Docs.html. The model chemistry includes the basic HO_x-NO_x-CH_4 gas phase chemistry, NMHC chemistry, photolysis reactions, as well as heterogeneous losses for all soluble species. A detailed listing of reactions and rate coefficients has been recently provided by *Crawford et al.* [1999a]. The NMHC chemistry was taken from the condensed mechanism of *Lurmann et al.* [1986]. It was further modified, however, to include: (1) updated rate coefficients, (2) additional reactions to reflect the low-NO_x environment encountered during the PEM-Tropics missions (e.g., formation of organic peroxides), and (3) explicit chemistry for some species previously "lumped" into families (e.g., acetone, propane, and benzene) in the Lurmann mechanism.

Photolysis rate coefficients were evaluated either using a DISORT 4-stream implementation of the NCAR Tropospheric Ultraviolet-Visible (TUV) radiative transfer code, [*Stamnes et al.*, 1988] (modified by S. Madronich, private communication, 2001) or were provided from spectroradiometer measurements, e.g., [*Lefer et al.*, this issue]. (A more detailed description of the photolysis rate coefficient calculations can be found in *Crawford et al.* [1999b].)

Of the 12 nonhydrocarbon photolysis rate coefficients used in the current analysis, for all but one of these the quantum yield and absorption cross section data were those reported by *DeMore et al.* [1997]. The exception was the quantum yield data for $O(^1D)$ formation where the more recent quantum yield data of *Talukdar et al.* [1998] were used. All model-calculated photolysis rate coefficients were adjusted to reflect the actual solar/cloud conditions encountered during an individual flight. This was achieved using a "cloud correction factor" (CCF) that was applied to each individual data run. (The quantity CCF has been previously defined by *Davis et al.* [1993, 1996], *Chen* [1995], and *Crawford et al.* [1996, 1997b, 1999b].) Its value was defined from Eppley UV measurements or from spectroradiometer determinations of $J(NO_2)$. In both cases comparisons were made between actual field derived values and those estimated from the radiative transfer model for clear sky conditions. The same CCF value was applied to all J-values and was assumed to be constant over the solar day. For the PEM-Tropics A and B field studies the average CCF value was ~ 0.93.

Model calculations were typically constrained by observations of O_3, CO, NO, temperature, dew point, and pressure. For PEM-Tropics B they were also constrained with acetone measurements. Due to the more limited measurements for NMHCs, H_2O_2, and CH_3OOH, the observational data for these species was not used to constrain our standard model runs. They were, however, used in several sensitivity test runs.

3.2. Three-Dimensional Model

As noted earlier, in years past, 3-D generated global profiles of OH have been the primary basis for assessing the global chemical consequences of OH chemistry. These profiles were developed by constraining the model with chemical precursor levels. Unlike box models, however, where precursor input levels are based on direct observations, the inputs to 3-D models are generated from emission inventory data in combination with an appropriate wind field for diluting and transporting the emissions.

The global 3-D model used in this comparison is that previously described by *Wang et al.* [1998a]. This model uses a spatial resolution of 4° latitude by 5° longitude. In the troposphere, it is subdivided into seven vertical layers, the upper boundaries of which are at approximately 0.5, 1.2, 2.6, 4.7, 7.2, 10.1, and 14 km. For purposes of comparison with the observations and box model results, median values of OH were estimated over the same longitude range as specified below for the experimental database. In addition, the 24 hour averaged OH values, typical output for a 3-D model, were all scaled to high noon values using appropriate diurnal averaging factors. (The latter factors were derived from box model runs as a function of latitude, altitude, and season of the year.) The 3-D model also included a CCF; however, this was folded into the model estimated J-values using climatological cloud coverage values for the Pacific basin.

Transport in the 3-D model is driven by meteorological fields from a general circulation model developed at Goddard Institute for Space Studies [*Hansen et al.*, 1983]. The model simulates 15 chemical species or families including O_3, NO_x, N_2O_5, HNO_3, HNO_4, peroxyacetylnitrates, alkylnitrates, CO, ethane, ($\geq C_4$) alkanes, ($\geq C_3$) alkenes, isoprene, acetone, ($\geq C_4$) ketones, and H_2O_2. Emission inventory data included that associated with fossil fuel combustion [e.g., *Benkovitz et al.*, 1996], biomass burning, lightning [e.g., *Price and Rind*, 1994], and fertilizer use [*Yienger and Levy*, 1995]. Also included were isoprene and acetone emissions from vegetation based on the analysis of *Guenther et al.* [1995]. Dry deposition was computed with a resistance-in-series scheme as described by *Wesely* [1989]. Results from the 3-D model have been compared against long-term measurements of O_3 and CO and against aircraft measurements of NO, PAN, HNO_3, ethane, acetone, and H_2O_2 as presented by *Wang et al.* [1998b]. In general, they have compared favorably.

3.3. Approach

The current OH analysis has proceeded through several intermediate steps. The first of these involved dividing the PEM-Tropics A and B OH data into four data subsets. From PEM-Tropics A (fall season, August-September), two data subsets were identified and labeled as "central Pacific" (120°W to 180°W), and "eastern Pacific" (80°W to 100°W). Both involved data collected on the P-3B aircraft. The "eastern" data covered the latitude range of 14°S to 14°N. The central Pacfic data also had significant components in both the NH and SH, but spanded a much larger latitude range, i.e., 21°S to 21°N. (The authors note that a modest amount of additional OH data was recorded to the south of 14°S in the eastern Pacific, but these data were rejected because of low S/N ratios, reflecting instrument problems at the time.)

From PEM-Tropics B (spring season, March-April), the two data subsets that emerged were both located in the central Pacific. Both also had the same longitudinal coordinates as cited above for the PEM-Tropics A, central Pacific. The major difference between the two involved the respective latitude ranges (e.g., 28°S to 35°N versus 35°S to 28°N) and the sampling platform/OH instrument employed to collect the data.

Having subdivided the two PEM-Tropics field studies into four data subsets, six additional steps were taken to get the

model results and observational data into their final forms. These involved: (1) filtering the observational OH data to identify only those data collection times that had concurrent values for the four precursor species NO, O_3, CO, and H_2O; (2) filtering all OH observational data from step 1 to identify outlying CCF values (i.e., only values between 0.6 and 1.35 were considered); (3) scaling all observational OH values to highnoon; (4) selecting only highnoon OH values from each TD box model run; (5) compiling all observational and model OH values, as well as precursor data, into latitude/altitude bins 7°x 0.5 km; and (6) estimating the median value for each latitude/altitude grid box using all available data in each grid box.

Based on the above processing scheme, the final data subsets that emerged covered a latitude range of 30 to 60 degrees and an altitude range of 8 to 12 km. Approximately 78% of all grid boxes in the four data fields contained three or more data points; 68% had five or more points. Although there was some concern about using grid boxes having fewer than three data points (22%), upon dropping these boxes we found no significant shift in any previously identified trend in the distribution plots. Thus, these grid boxes were left in since they provided additional visual continuity to the grid plots.

Of the six processing steps cited above, step 4, involving scaling of the OH observational data, was determined to have the highest potential for introducing a bias in the results. Our initial thinking for minimizing this problem involved considering only those OH values recorded within a very narrow solar window, i.e., those centered around highnoon. This approach was rather quickly rejected, however, in that it reduced the total available OH population to a statistically unacceptable small number. The scaling of all observations maximizes the available data, but presents the new problem of potentially generating large scaling errors for the high zenith angle data. The error increases rapidly with increasing zenith angle both due to the lower precision of the measurements (reflecting lower concentration levels of OH), and due to the absolute magnitude of the scaling factor with higher zenith angles, e.g., amplifying any precision error. To minimize this problem, as discussed in greater detail in the text below, it was determined that an additional filtering restriction was needed as related to zenith angle, namely, values were rejected that were > 60°.

But the scaling process itself raised still other issues. The most important of these being the selection of an algorithm as a basis for scaling. For this study, we chose to use the availability of the diurnal profile data generated on the P-3B as the initial

Table 1. Comparison of OH Scaling Factors as Derived From Observations and Model

Alt/Flt	OH scaling factor: OH_{noon}/OH(LST)									
	LST[a]	800	900	1000	1100	1200	1300	1400	1500	1600
0.3 km	SZA[b]	62.4	48.4	35.1	23.7	18.4	23.7			
Flight	Obs.[c,d]	4.39	1.80	1.26	1.06	1.00	1.03			
16	Model[e]	4.25	1.78	1.29	1.06	1.00	1.08			
	M/O[f]	0.97	0.99	1.02	1.00	1.00	1.05			
1.4 km	SZA	62.4	48.4	35.1	23.7	18.4	23.7	35.1		
Flight	Obs.	5.67	2.61	1.51	1.10	1.00	1.15	1.65		
16	Model	3.78	1.85	1.26	1.05	1.00	1.06	1.32		
	M/O	0.67	0.71	0.83	0.96	1.00	0.92	0.80		
3.0 km	SZA					25.6	29.4	38.9	50.9	64.1
Flight	Obs.					1.00	1.06	1.33	1.98	3.51
14	Model					1.00	1.06	1.27	1.82	3.54
	M/O					1.00	1.00	1.05	1.09	0.99
5.5 km	SZA					25.2	29.2	38.8	50.9	64.0
Flight	Obs.					1.00	1.06	1.25	1.64	2.41
14	Model					1.00	1.04	1.18	1.51	2.40
	M/O					1.00	0.98	0.95	0.92	1.00

[a] Local Sun time.
[b] Solar zenith angle.
[c] Observed OH scaling factor derived from empirical fit of diurnal OH observations.
[d] Observed OH scaling factors for observational time periods only.
[e] Model OH scaling factors derived from model calculated OH profiles.
[f] Ratio of model OH scaling factor to observed scaling factor.

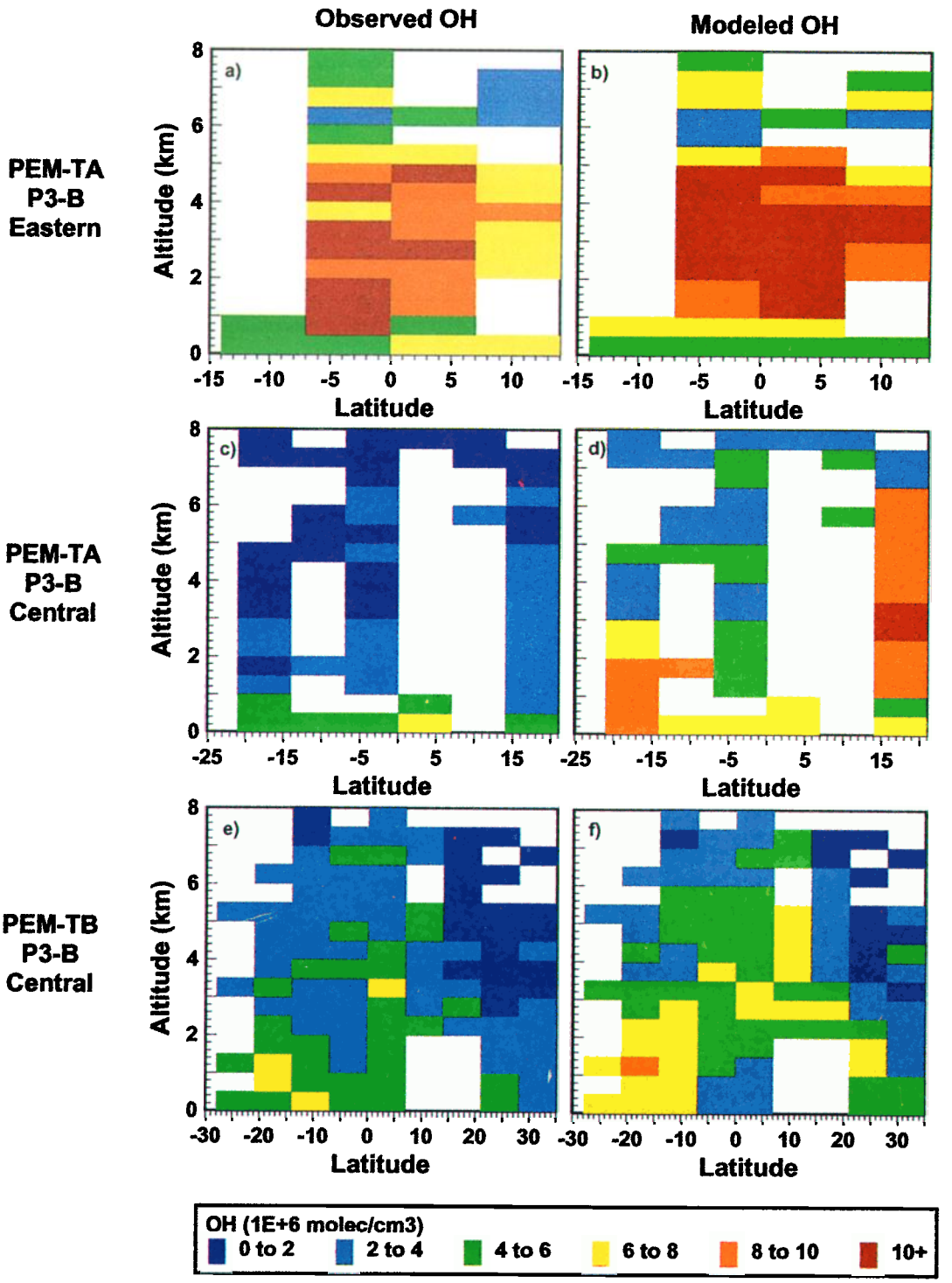

Plate 1. Median values of OH at high-noon estimated from P-3B observations. Data are binned every 7° of latitude and 0.5 km in altitude. (a) PEM-Tropics A OH observational values for the eastern Pacific (80°W to 100°W) during fall season; (b) PEM-Tropics A OH box model values for the eastern Pacific during fall season; (c) PEM-Tropics A observational values for the central Pacific (120°W to 180°W); (d) PEM-Tropics A box model values for the central Pacific; (e) PEM-Tropics B OH observational values for the central Pacific during spring season; (f) PEM-Tropics B box model values for the central Pacific during spring season.

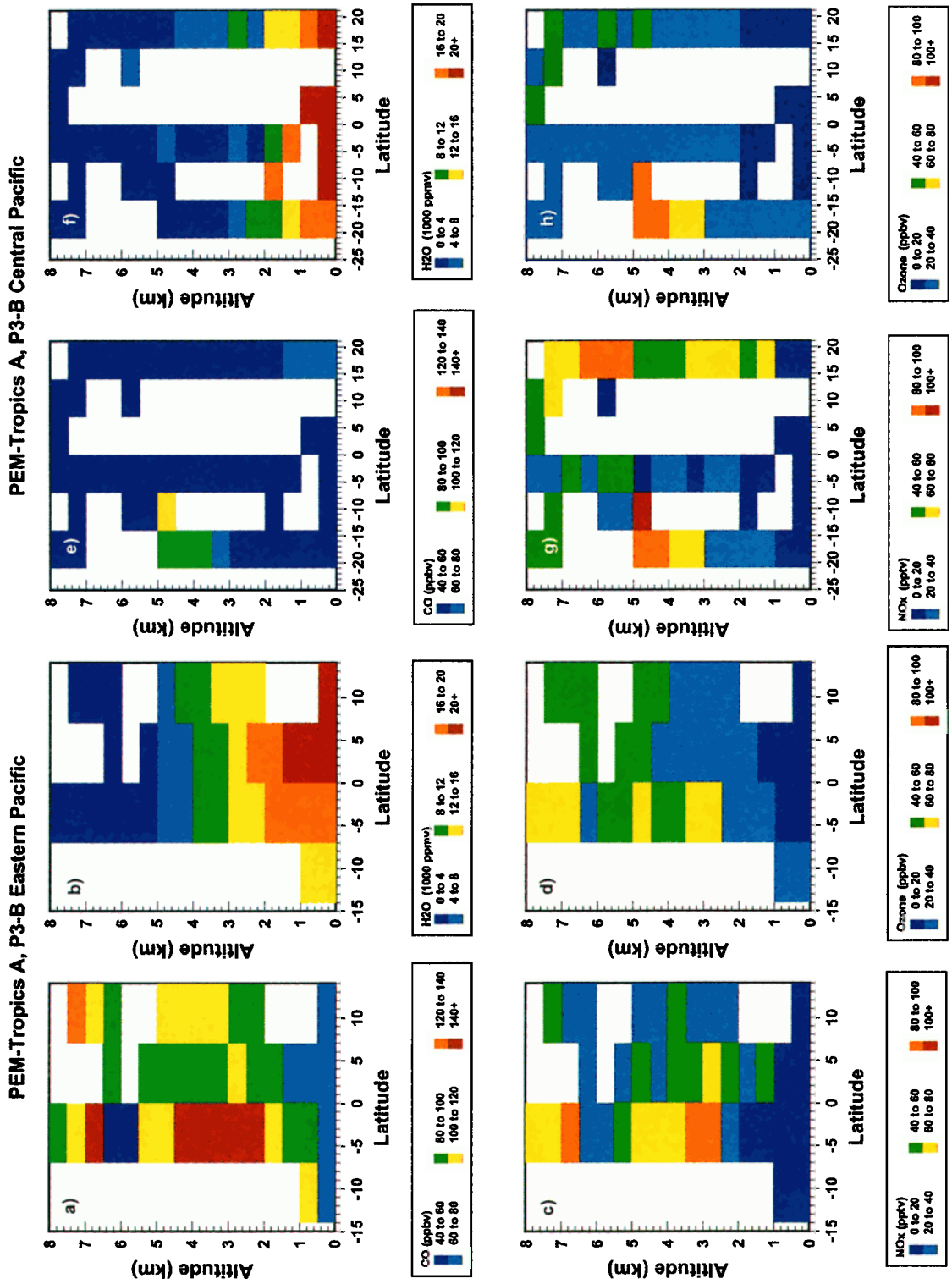

Plate 2. Median values of photochemical precursors estimated from P-3B observations during the fall season. Data are binned every 7° of latitude and 0.5 km in altitude. (a) CO, eastern Pacific; (b) H_2O, eastern Pacific; (c) NO_x, eastern Pacific; (d) O_3, eastern Pacific; (e) CO, central Pacific; (f) H_2O, central Pacific; (g) NO_x, central Pacific; and (h) O_3, central Pacific.

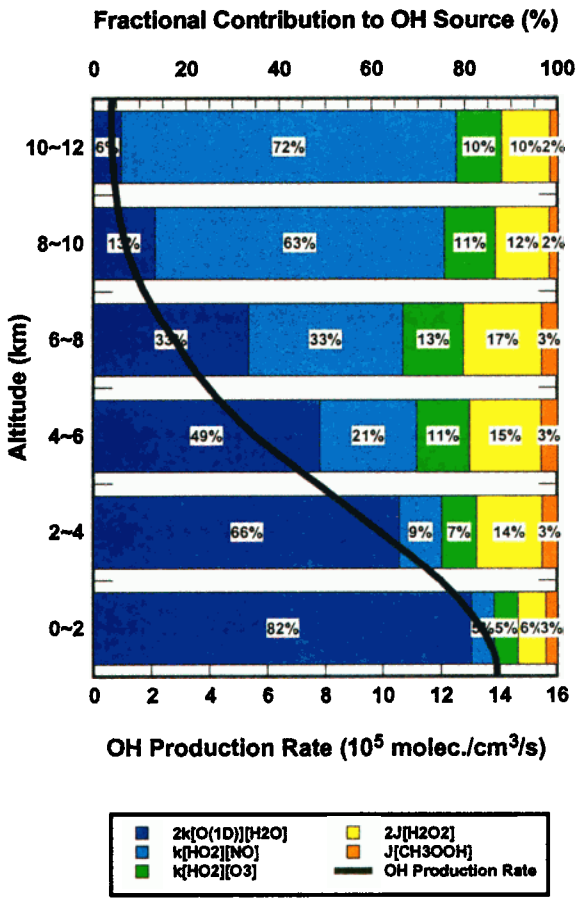

Plate 3. Model-estimated OH production rate at tropical latitudes with fractional contributions from primary and recycled sources. Model runs are based on PEM-Tropics A and B data recorded in the central Pacific.

basis for scaling. Diurnal OH profile data were generated during several missions in which an Eulerian sampling strategy was employed. Specific missions using this strategy included: 7, 8, 11, 14, and 16. These missions covered an altitude range of 0.3 to 5.5 km. During each, sampling runs were executed repeatedly at three preselected altitudes. Nearly the same geographical coordinates were then targeted for repeated flight legs at these altitudes. Because of the equatorial setting, there typically was an ~800 km fetch associated with each of these Eulerian sampling sites. Thus, variations in precursor levels at each altitude were typical less than 15%.

In our analysis of the above data, the experimentally based diurnal OH profiles were used to determine the rate of roll-off of OH on each side of highnoon relative to that predicted by the box model calculations. Thus, the ultimate goal was that of developing a "relative" scaling factor defined in terms of model generated values. As shown in Table 1, representative data recorded at altitudes of 0.3, 1.2, 1.4, 3.0, and 5.5 km indicates that the level of agreement was typically 20% or better, with 33% being the worst case. As expected, the level of agreement decreased with increasing solar zenith angle, leading to our final decision to reject all data with zenith angles > 60°. The level of agreement was also found to be better for data generated in the afternoon than in the morning. At present, we have no simple explanation for this difference. However, given the general agreement found in these results, it was concluded that using a relative scaling factor based on the model simulations would not introduce a significant systematic model bias into the observational data.

Of the data scaled, approximately 85% had zenith angles ≤ 50°, and 66% had angles ≤ 40°. Thus, we estimate that the potential error resulting from the scaling of the OH data to be less than 20%.

4. Observations, Model Results, and Discussion

OH observations were recorded during two seasons (i.e., fall and spring), over two geographical regions (the eastern and central Pacific), using two aircraft platforms (P-3B and DC-8), and using two different OH instruments (SICIMS and ATHOS). Below we present these data and the modeling results as subdivided according to field program, season, geographical region, and aircraft platform.

4.1. PEM-Tropics A Fall Season

The two geographical regions examined during PEM-Tropics A can best be identified in terms of their respective longitude coordinates. The eastern Pacific region was bracketed by 80°W to 100°W; whereas, the central region covered the range of 120°W to 180°W. During PEM-Tropics A only the P-3B aircraft was instrumented with an OH sensor. However, both aircraft had a complete complement of instruments for recording the levels of photochemical precursor species.

4.1.1. Eastern Pacific P-3B. Shown in Plate 1a are the noontime scaled OH data recorded in the eastern Pacific. They are unusual in that the levels are considerably higher than what one might expect for a remote Pacific area (see sections 4.1.2, 4.2.1, and 4.2.2). For example, several mid-altitude grid boxes show noontime OH values reaching in excess of 1 x 10^7 molecules cm^{-3}. Equally interesting is the observation that the trend in these data reveals that mid-altitude values are significantly elevated (factor of 2) over those in the BL. Both observations appear more reasonable, however, when placed in the context of the photochemical precursor profiles (Plates 2a-2d). They show the presence of highly elevated levels of H_2O, O_3, NO_x, and CO. As presented in Plate 3, both H_2O and O_3 are critical to the primary production of OH. Similarly, NO_x and O_3 are potentially major sources of recycled OH via HO_2 radicals. From Plate 2c, NO_x values at mid-altitudes are shown exceeding those in the BL by factors of 3 to 9. At levels of 50+ pptv the HO_2/NO recycling reaction becomes a major source of OH. When combined with enhancements in primary production due to elevated O_3 and H_2O, this highly perturbed marine environment leads to enhancements in OH production of factors of three. Thus, even with the indicated increase in CO by factors of 1.5 to 2 (increasing OH loss), the predicted OH concentration is well above that expected for a remote tropical marine setting.

The source of the elevated H_2O, O_3, NO_x, and CO in the eastern Pacific region has been addressed by *Fuelberg et al.* [1999]. These authors have pointed out that during the fall 1996 campaign the primary source of air at 3 to 6 km off the west coast of northern South America was from South America itself. As a result, it was strongly influenced by biomass burning. The latter conclusion has been well documented in yet another PEM-Tropics A investigation by *Olson et al.* [1999], and references therein.

The box model results shown in Plate 1b are seen as in excellent agreement with the observations. However, a more

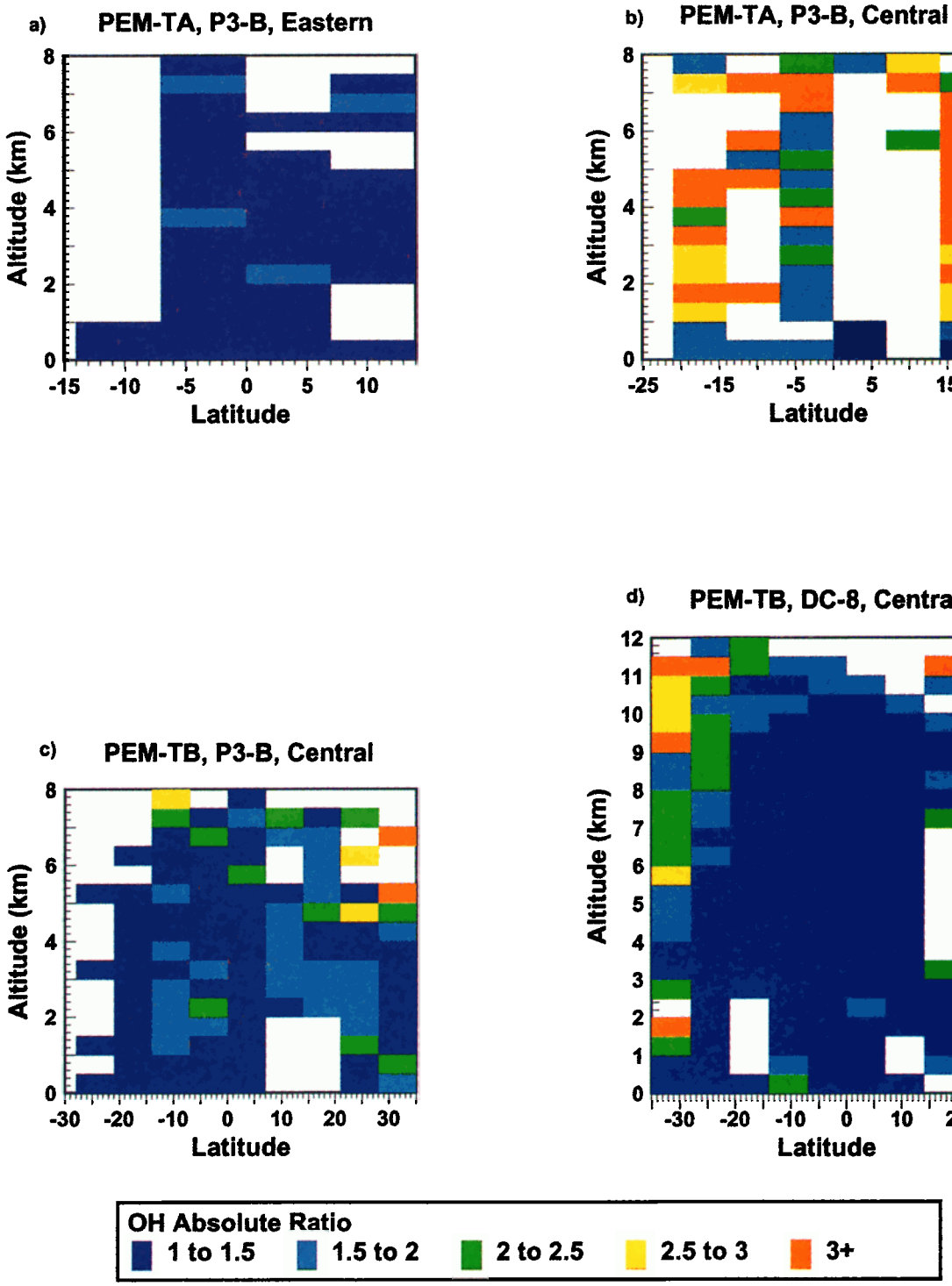

Plate 4. Comparison of model OH (OH_m) with observed OH (OH_o) values. The "goodness" of the comparison is expressed in terms of the ratio OH_m/OH_o or OH_o/OH_m, whichever is larger. Data are binned every 7° of latitude and 0.5 km in altitude. Ratios values are shown for: (a) P-3B observations, PEM-Tropics A, eastern Pacific (80°W to 100°W); (b) P-3B observations, PEM-Tropics A, central Pacific (120°W to 180°W); (c) P-3B observations, PEM-Tropics B, central Pacific; and (d) DC-8 observations, PEM-Tropics B, central Pacific.

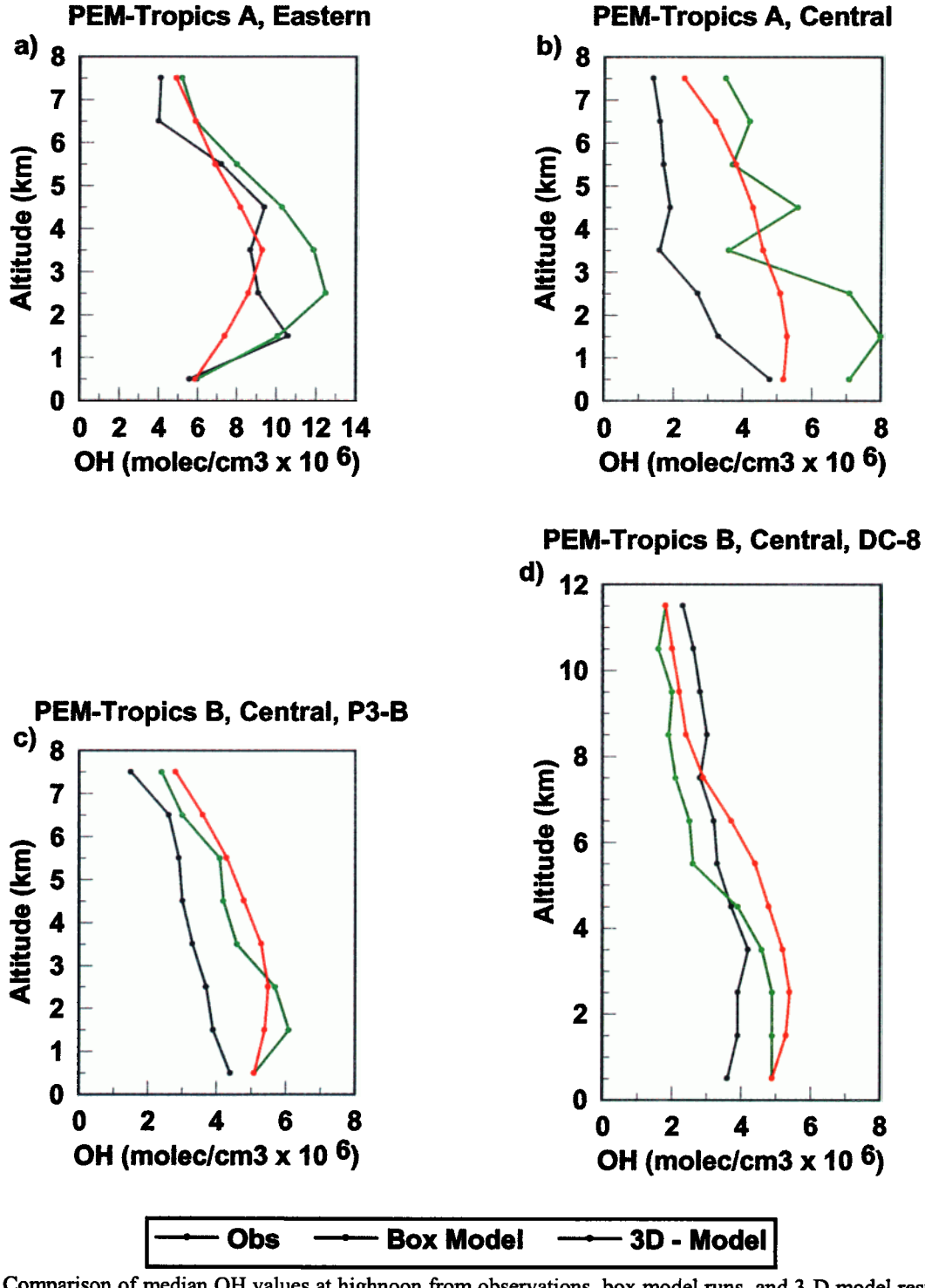

Plate 5. Comparison of median OH values at highnoon from observations, box model runs, and 3-D model results. Median values for each 1 km altitude zone are derived from data recorded over all latitudes. The 3-D model values are linearly interpolated with altitude and scaled to highnoon. (a) PEM-Tropics A, P3-B, eastern Pacific (14°S to 14°N, 80°W to 100°W), (b) PEM-Tropics A, P3-B, central Pacific (21°S to 21°N, 120°W to 180°W), (c) PEM-Tropics B, P3-B, central Pacific (21°S to 35°N, 120°W to 180°W), and (d) PEM-Tropics B, DC-8, central Pacific (35°S to 28°N, 120°W to 180°W).

quantitative comparison of these two data sets is presented in Plates 4a and 5a. In Plate 4a, the value of the OH ratio is shown plotted in the standard altitude versus latitude format. In this plot, as with similar ones to be shown later in the text, the value of the OH ratio has been estimated either from the "observed-to-model" or "model-to-observed" ratio, depending on which is larger. Thus, the intent here has been to attempt to show the absolute deviation between the model and observations. (Note, the issue of whether one has a systematic bias will be addressed later in the text.) What these results reveal is that for nearly 95% of the grid boxes containing data, the agreement is within a factor of 1.5, well within the limits defined by the combined uncertainties.

In Plate 5a, the median value for each 1 km altitude zone is plotted as a function of altitude. In this analysis, the median value has been defined by examining all data points over all latitudes within the targeted altitude range. These compiled results clearly indicate that for most altitudes the box model predictions are higher than the observations by factors of 1.5 or less. Also shown in Plate 5a are the similarly extracted median values for each altitude zone from the 3-D model simulations. Here one can see three different altitudes where the model and observations cross each other. As a result, the final overall agreement between the 3-D model predictions and observations is actually slightly better than that for the box model. The corresponding latitude/altitude profile reflecting the above cited 3-D results is presented in Plate 6. (Note, these 3-D data have been extracted from the model output data for the same longitudinal and latitudinal coordinates as specified earlier for the eastern Pacific.) As in the case of the box model results, it is quite apparent that the general trends seen in the observational OH data are nicely captured in the 3-D latitude/altitude profile.

4.1.2. Central Pacific P-3B. The observational OH data recorded during PEM-Tropics A for the central Pacific are shown in Plate 1c. Clearly, the values shown here are much closer to those expected based on previous OH observations in the central Pacific [*Eisele et al.*, 1996; *Mauldin et al.*, 1998, and references therein]. The maximum value observed (~ 6 x10^6 molecules/cm^{-3}) is seen occurring at the lowest altitude (0-1 km), but quickly drops to 1 to 3 x 10^6 molecules cm^{-3} as 3 km is reached. However, a quick comparison with the box model predictions (see Plate 1d) reveals considerable disagreement between the two. The level of disagreement is made even more evident in Plate 4b which shows a plot of the OH ratio as function of altitude and latitude. In this case, nearly 50% of the grid boxes are seen having values of 2.5 or higher. This is beyond the combined errors associated with the model and observations. Plate 5b also reveals that the higher ratio values are typical driven by higher model predicted OH values. The 3-D model results (Plate 6b) are also higher than the observations; however, values for the OH ratio are significantly lower than those derived from the box model calculations, e.g., 1.5 to 2.0. Thus, the 3-D results tend to split the difference between the box model results and the observations.

As seen in Plate 4b, the elevated box model predictions are primarily associated with the high values over two latitude bands: 14°N to 21°N, and 14°S to 21°S. In both cases, the high values occur above 1 km. In surveying the photochemical precursor plots (Plates 2e-2h), the most obvious species driving the higher model result is NO_x, although O_3 is also a small contributor. Both species promote increased primary production and enhanced recycling from the HO_2/NO and HO_2/O_3 reactions.

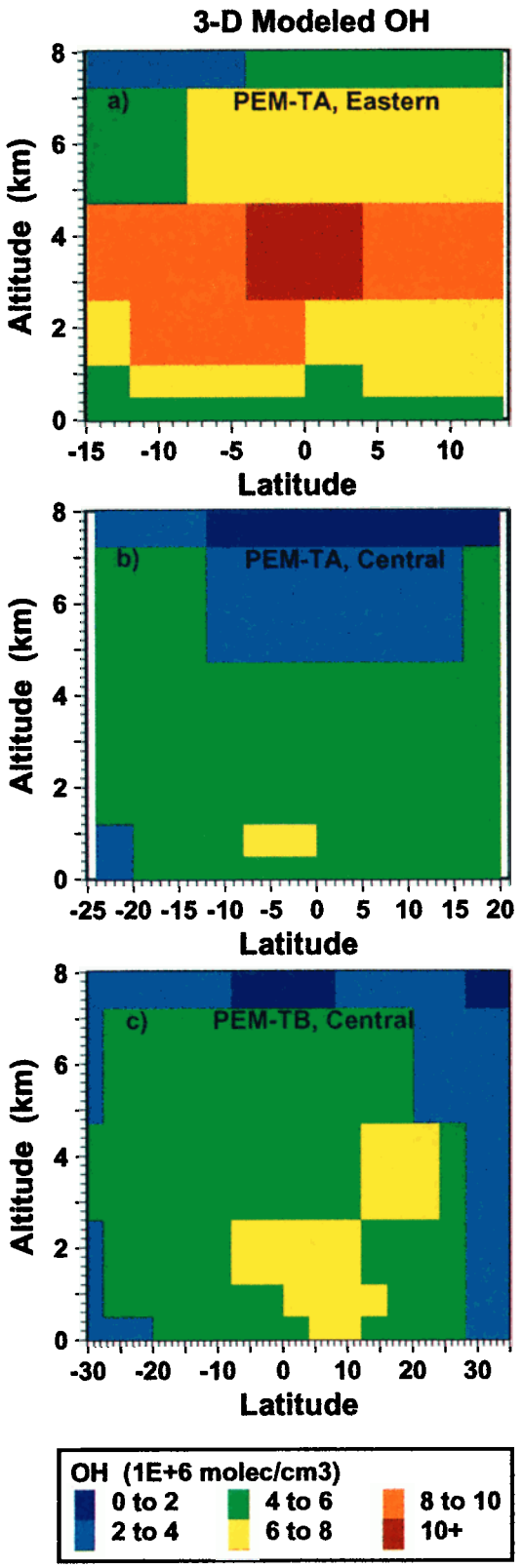

Plate 6. Highnoon scaled OH values estimated from 3-D model calculations. Values shown reflect the average OH concentration for the model latitude band of 4° and a vertical resolution defined by seven layers. The upper boundaries for these seven layers are ~ 0.5, 1.2, 2.6, 4.7, 7.2, 10.1, and 13.5 km. (a) PEM-Tropics A, eastern Pacific (80°W to 100°W) during fall season; (b) PEM-Tropics A, central Pacific (120°W to 180°W) during fall season; and (c) PEM-Tropics B, central Pacific during spring season.

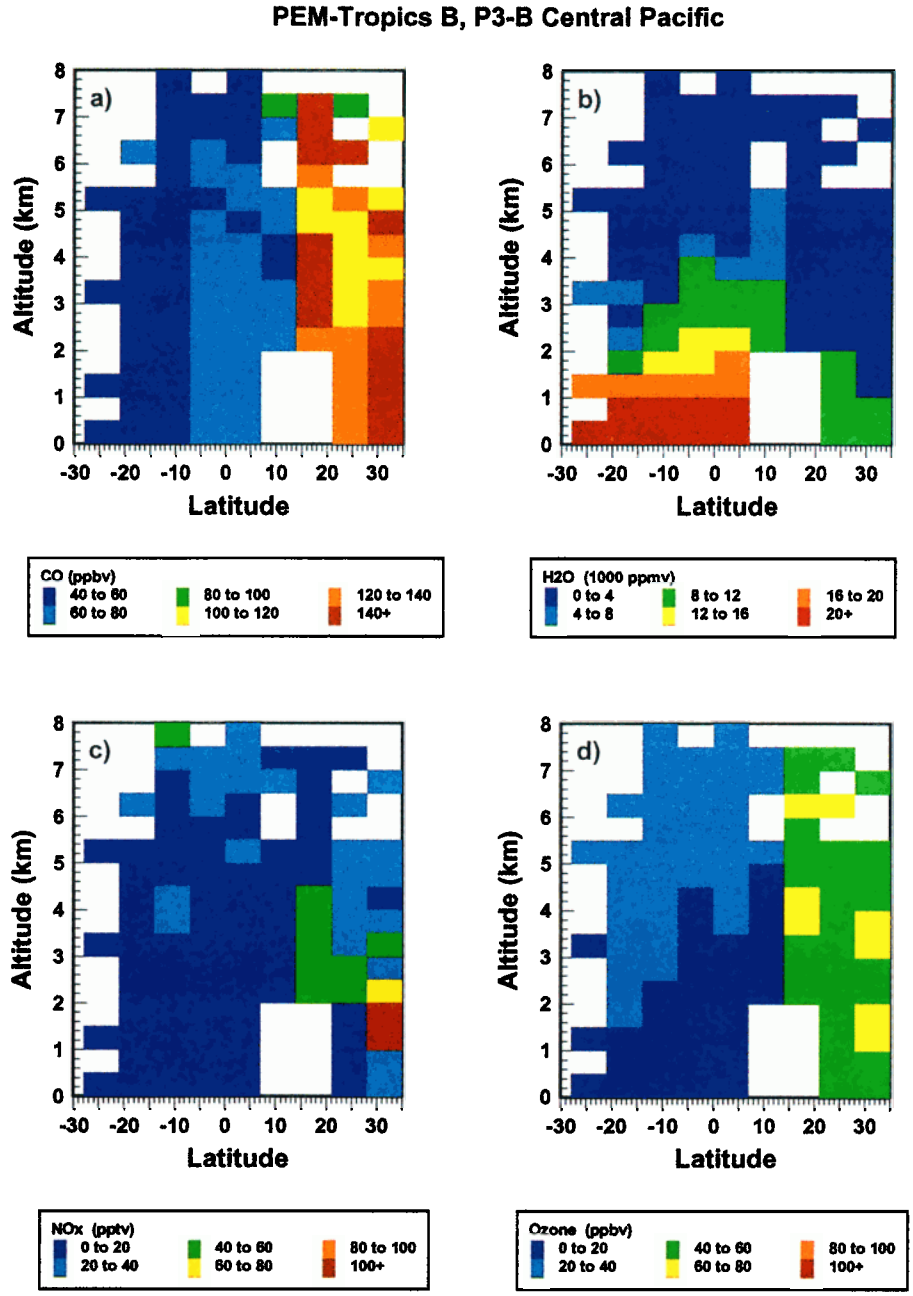

Plate 7. Median values for photochemical precursors as estimated from P-3B spring observations in the central Pacific (120°W to 180°W). Data are binned every 7° of latitude and 0.5 km in altitude. (a) CO, (b) H_2O, (c) NO_x, and (d) O_3.

Considering the magnitude of the difference between the model results and observations, it is difficult to side step the question why this might be. As already noted, nearly 50% of the box model results are outside of the combined error of the observations and model calculations. Possible problem areas include shortcomings in the model mechanism, large unidentified errors in the precursor observations, unknown sources of error in the OH observations, or some combination of all three. This setting is in strong contrast to that in the eastern Pacific where the high degree of correspondence between the box model predictions and observations would suggest that none of the above possibilities is likely.

Upon further reflection, however, still a fourth possibility emerges, that involving the role of NMHCs and peroxide species. Recall, in our original set of model runs we did not constrain the model with either NMHCs or peroxide species. The reason for this was the absence of data at 1 min. time resolution plus the fact that these data were available only sporadically. To explore how the addition of these species might shift the model results, sensitivity tests were carried out on all data blocks. In these simulations, model values were compared with and without constraints from measurements of NMHCs and peroxides. The number of constrained runs was ~ 50% of the total. The results showed that NMHCs had, at most, a 3% effect on calculated OH levels. The peroxide influence was somewhat larger, but was still limited to only 2 - 10%.

The 2σ uncertainty in the box model simulations has previously been cited as ± 60% [*Davis et al.*, 1993; *Crawford et al.*, 1999a; *Chen et al.*, 2001]. This error was estimated from Monte Carlo calculations using the cited uncertainties in all "*J*" and "*k*" values. In a perfect world where all systematic errors in these "constants" were removed, this means that any new model calculation would be either higher or lower than the current results. Thus, assuming that the shift brought about by having accurate rate coefficients was large enough, one could argue that it might be possible to remove the model over-prediction at 14°N to 21°N and that at 14°S to 21°S. Then, the OH results at all other latitudes in the central Pacific would most likely be in error as would all the eastern Pacific results. However, what the above scenario does not address is the possibility that critical chemical processes (not included in our mechanism) might have been active in some regions of the Pacific but not in others. Although clearly possible, the good agreement seen in the other two central Pacific data subsets, see sections 4.2.1 and 4.2.2, would seem to make the latter hypothesis unlikely.

As mentioned earlier, still another possibility could involve measurement errors. For example, during PEM-Tropics A substantial differences were found in the NO_x levels observed in the central Pacific as measured on the P-3B versus the DC-8, the DC-8 being much lower. This shift was not observed for any other species. Suffice it to say, at this time it is not possible to rule out errors in one or more of the critical photochemical measurements, including OH itself; however, it is also not possible to totally exclude mechanistic shortcomings in the model.

4.2. PEM-Tropics B Spring Season

During PEM-Tropics B, OH observations were recorded on both the P-3B and DC-8 aircraft. The major geographical region of focus for both aircraft was the central Pacific as defined earlier in the text.

4.2.1. Central Pacific, P-3B. The central Pacific P-3B data are those shown in Plate 1e. Quite noticeable here is the similarity between these observations and those examined earlier in Plate 1c, i.e., PEM-Tropics A, central Pacific. In both cases the highest OH concentrations are at the lowest altitude sampled, reaching values of 5-7 x 10^6 molecules cm^{-3}. However, unlike PEM-Tropics A, values tend to remain relatively high up to 7.5 km. This "seasonal shift" is particularly clear in the case of the SH where the difference between the NH and SH is seen reaching factors of 2 or greater for some altitudes. As shown in Plate 7b, one of the more important contributing factors to this SH trend is the elevated level of water. As discussed earlier, Plate 3 indicates that even at altitudes of 6-8 km primary production of OH via the $O(^1D)/H_2O$ reaction can account for nearly one third of the total OH formation. As discussed by *Fuelberg et al.* [this issue], the enhanced SH H_2O level during PEM-Tropics B was a direct result of increased levels of deep convection (i.e., east of the dateline).

The influence of elevated SH H_2O levels has been nicely captured in the modeling results shown in Plate 1f. Here OH values in the 4 to 6 x 10^6 molecules cm^{-3} range are shown up to altitudes of 6 km. By comparison, NH values tend to be lower even though Plates 7c and 7d reveal the presences of elevated O_3 and NO_x. Given the fact that the model results shown in Plate 3 indicate the important role played by NO_x and O_3 in OH formation, it might be expected that enhanced levels of these species would drive up OH levels. But Plate 1f shows this not happening for latitudes above 15°N. The reasons for this involve the two critical precursors, CO and H_2O. As shown in Plates 7a-7b, at low to mid-altitudes CO levels were quite high and H_2O was quite low, relative to SH latitudes. Thus, this is one of those cases which illustrate how OH can sometimes demonstrate an apparent insensitivity to significant shifts in photochemical precursor levels. This can happen due to the offsetting effects from several precursor levels changing at the same time. The effects from such shifts can also be dampened by the nonlinearity of the OH chemistry itself.

Using the same approach taken for the PEM-Tropics A results, Plate 4c reveals that nearly 65% of the grid boxes for the central Pacific (PEM-Tropics B) show agreement to within a factor of 1.5. Another ~20% show agreement to within a factor of 1.5-2.0. But as shown in Plate 5c, the model predictions tend to be modestly higher than the observations. Even so, these results are in sharp contrast to those from PEM-Tropics A, central Pacific (section 4.1.2).

The 3-D model results corresponding to the time period of PEM-Tropics B are shown in Plates 5c and 6c. From Plate 6c it can be seen that regions showing some of the highest OH values tend to be in the NH; whereas, the observations as well as the box model results have their highest values in the SH. In spite of this small shift, the overall results from the 3-D model appear to be in reasonably good agreement with both observations and box model results. For example, Plate 5c reveals that the OH profile derived from the 3-D results typically exceeds those based on the observations and box model, but the level of agreement is still within a factor of 1.3.

4.2.2. Central Pacific DC-8 OH Data. The gridded DC-8 OH observations are shown in Plate 8a. Quite striking is the fact that this profile shows very little variability as a function of latitude. It also reveals a very modest trend with altitude. For example, at most latitudes the maximum value occurs between 3 and 5 km (e.g., 4-6 x10^6 molecules cm^{-3}). Somewhat lower values are shown for the BL and the upper free troposphere (i.e., 2-4 x10^6 molecules cm^{-3}). By contrast, the box model results displayed in Plate 8b tend to show higher OH values at low altitudes (4-8 x

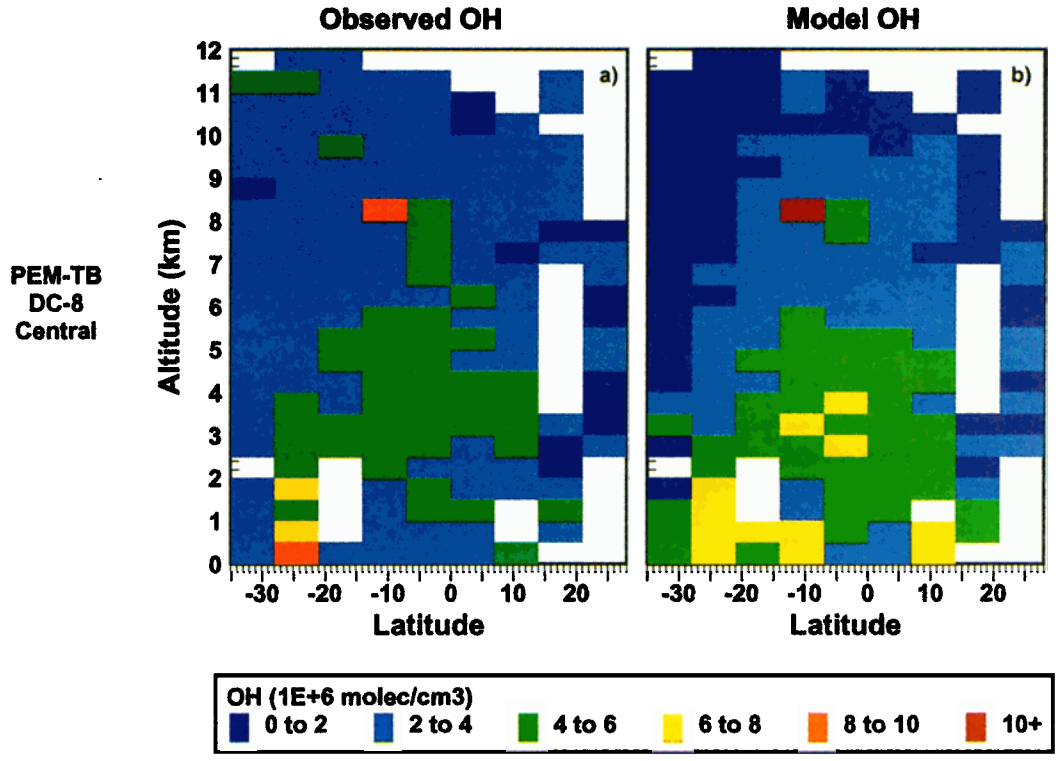

Plate 8. Median values of OH at high-noon estimated from the PEM-Tropics B DC-8 spring observations in the central Pacific (120°W to 180°W). Data are binned every 7° of latitude and 0.5 km in altitude. (a) OH observations; and (b) OH box model values.

10^6 molecules cm^{-3}) with a general trend of decreasing values moving toward high altitudes (0-4 x 10^6 molecules cm^{-3}). The differences between model and observation, however, are actually quite modest as revealed in the more quantitative comparison given in Plate 4d. Here the OH ratio values indicate that ~80% of the grid boxes have values ≤ a factor of 1.5. Another ~10% are within a factor of 1.5-2.0. Plate 5d indicates that the good agreement between model and observations has an interesting trend associated with it, namely, the model value crosses the observational value at an altitude of ~ 4.5 km, the model giving the higher value at low altitudes.

Upon examining the DC-8 precursor plots shown in Plates 9a-9d, it is quite apparent that the box model results have been more strongly influenced by the high H_2O levels at low altitudes (i.e., 0 to 4 km) than is reflected in the observations. Equally important are the significant increases shown in O_3 for altitudes above 3.5 km. As discussed earlier, enhanced O_3 can promote both enhanced OH primary production as well as recycling of OH via the HO_2/O_3 reaction. At 8 km and above, Plate 3 indicates that recycled OH actually becomes the dominant source, most of which is attributed to the HO_2/NO reaction. As shown in Plate 9c, some of the enhancements seen in NO_x above 8 km were reflected in the modeled OH. Of particular interest is the NO_x hot spot at 0°- 14°S and 8 km. The enhancement here is nicely captured not only in the model but also in the observations, as one would expect. By contrast, at still higher altitudes (11 -12 km), especially in the SH, the presences of elevated NO_x and O_3 levels is not seen correlated with elevated OH. In this case the influence of O_3 and NO_x appears to have been offset by the presence of very low H_2O levels. It is also noteworthy that at these higher altitudes acetone photolysis begins to contribute significantly to HO_x production.

The 3-D model results are shown along with those from the box model in Plate 5d. Here it is seen that at all altitudes the 3-D results are larger than those derived from the box model; but this difference becomes quite small (<20%) for altitudes <1.5 and >8.5 km. It follows that the general altitude trend in 3-D model results is also quite similar to those generated from the box model calculations. The most noticeable feature of the 3-D results, relative to the observations, is that the crossover point where 3-D values become lower than the observations occurs at a higher altitude than for the box model. The box model crosses at ~ 4.5 km while the 3-D crossover altitude is closer to 7.5 km.

4.2.3. Central Pacific comparison of P-3B and DC-8 OH Data. Although the P-3B and DC-8 aircraft were both in the field at the same time, they flew on the same days only 50% of the time. Furthermore, even when flying on the same days, the geographical and altitudinal coverages of the two flight tracks typically did not overlap. This reflects differences in aircraft operating ceiling, aircraft range, and on some occasions different scientific objectives. Even so, the general uniformity of the tropical Pacific, as evidenced in the model results and observations, was sufficiently high that one might expect the OH levels observed by the two aircraft to be similar. In fact, as revealed in Plates 1e and 8a, for the common latitude range of 21°S to 28°N, this is generally seen to be true. Typical OH values on both aircraft range from 2 to 6 x 10^6 molecules cm^{-3}. The most significant area of disagreement is seen in the respective altitude trends. The P-3B data show the largest values at altitudes below 2 km, with a general trend of decreasing values up to 8 km. Although the DC-8 database also shows a few grid boxes with large OH values below 2 km, this aircraft's profile reveals the largest block of high values to be between 2 and 6 km.

The photochemical precursor plots for the two aircraft (Plates 7a-7d and Plates 9a-9d), show a rather high level of

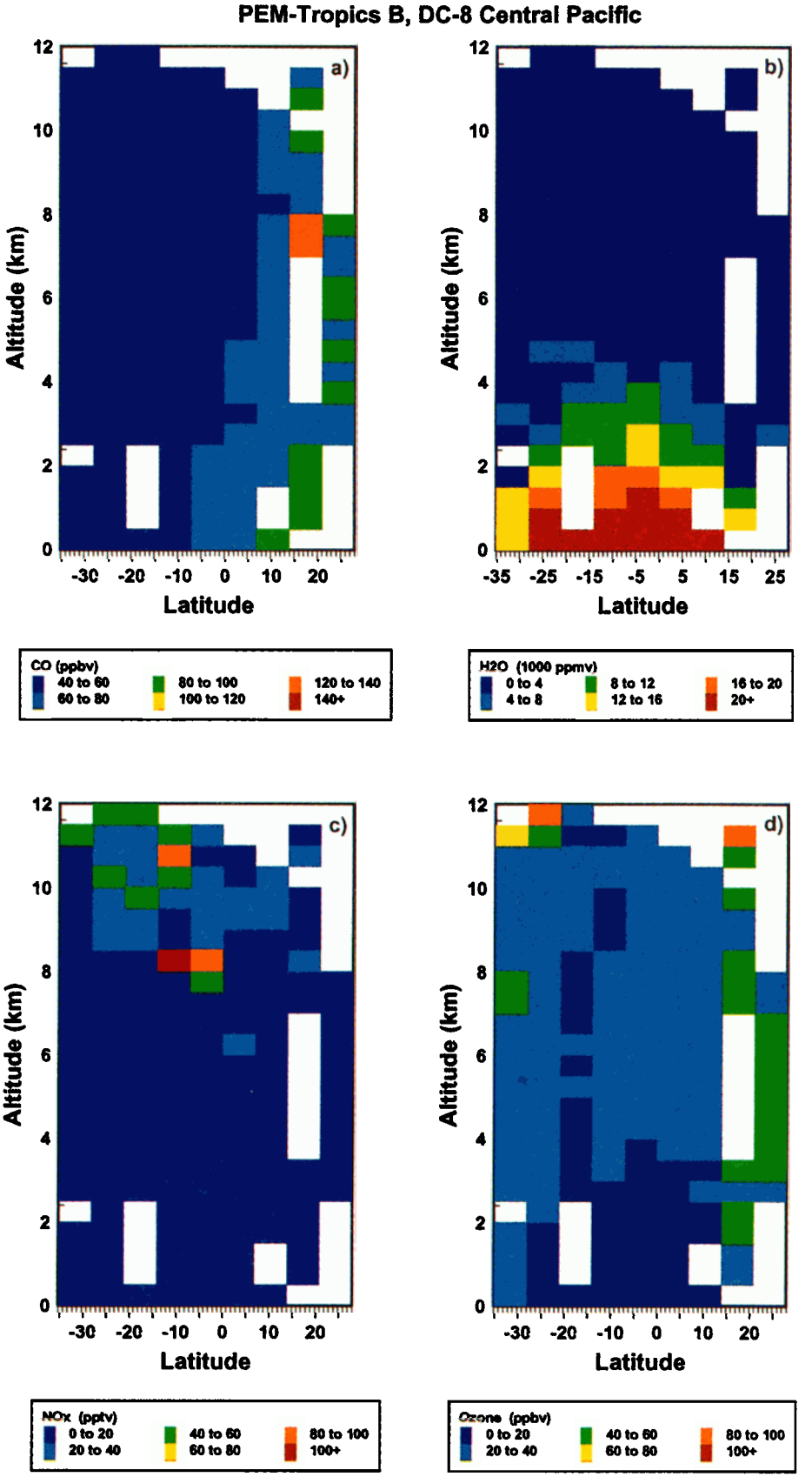

Plate 9. Median values of photochemical precursors estimated from DC-8 spring observations in the central Pacific (120°W to 180°W). Data are binned every 7° of latitude and 0.5 km in altitude. (a) CO, (b) H_2O, (c) NO_x, and (d) O_3.

correspondence for latitudes limited to 28°S to 15°N. Farther to the north significant differences are seen in NO_x, CO, and O_3, with the P-3B recording the higher values. For CO this enhancement is nearly a factor of 2; whereas, for NO_x it ranges from factors of 2 to 4. As noted in earlier discussions, this same NH zone also had some of the lowest H_2O levels. As a result, both aircraft report some of their lowest OH values in this region (i.e., 0-4 x 10^6 molecules cm^{-3}).

A more quantitative assessment of the two aircraft OH databases is presented in Plate 10. Here the range of latitude used to evaluate each aircraft's data was restricted to the common latitude range of 21°S to 28°N. These results indicate that although the median values of OH estimated for each altitude zone are relative close (typically < factors of 1.6), the altitude trend recorded by each instrument differed significantly. P-3B OH levels are seen starting out in the boundary layer at their maximum and then falling at a significant rate with increasing altitude. By contrast, the DC-8 OH data start in the boundary layer at less than their maximum, slowly increase to an altitude of 3.5 km, and finally, slowly decreases up to 7.5 km and above. Thus, the two aircraft profiles are seen crossing at ~2.5 km. Although the differences cited are well within the combined errors for each instrument, there remains a strong indication that an altitude bias may exist between the two techniques. When assessed, however, in the context of the larger geographical region analyzed (the central Pacific), one would be more inclined to argue that the level of agreement between these different techniques is really quite encouraging. (A more detailed flight by flight analysis of OH observations recorded on the two aircraft is presented in a companion paper by *Eisele et al.* [this issue].)

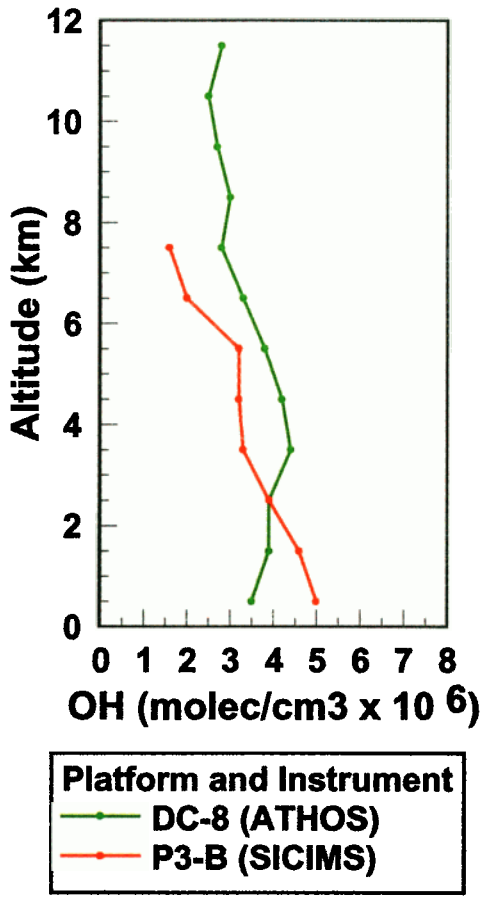

Plate 10. Comparison of P-3B OH observations with those recorded on the DC-8. All observational data are scaled to highnoon. Medians have been estimated from all data recorded over the latitude range of 21°S to 28°N and for altitude blocks of 1 km.

5. Summary and Conclusions

Reported here are OH observations and model results based on data recorded during NASA's PEM-Tropics A and B airborne field campaigns. These two programs had as their major geographical focus the central Pacific Ocean (120°W to 180°W). Extensive OH data were recorded for both the fall (August-September) and spring (March-April) seasons. In addition, during PEM-Tropics A, OH data were recorded in the eastern Pacific (80°W to 100°W). For the spring campaign, both the DC-8 and P-3B aircraft measured OH but using different OH instruments. The SICIMS instrument was employed on the P-3B and the ATHOS instrument on the DC-8.

In comparing the results from these two field studies against models and each other, it has been recognized that, unlike most other atmospheric species, a meaningful comparison of OH requires the availability of other supporting data. In previous OH comparison work, statistical evaluations of point-to-point comparisons for model results and observations have typically been carried out. This has generally allowed for a determination of the general consistency between measured and simulated values. However, because of the short lifetime and strong diel variability in OH, these individual measurements have not been very useful in generating a large-scale regional picture of OH. The latter is of considerable interest in that it can form the basis for a comparison with OH global simulations. Here we have used a scaling algorithm that has provided a means for converting individual OH observations into an equivalent high-noon value. This, in turn, has permitted our converting nearly the entire PEM-Tropics A and B OH observational data bases into a geographical altitude/latitude grid map. The latter has then been compared with both box model and 3-D model results. The weakness of this approach is quite apparent in that single campaign data are being used to create a regional picture. In fact, single campaign observations provide only a short term chemical snap shot of the region. Thus, their representativeness in making comparisons with 3-D model results may still be questioned.

The results from our analyses have revealed that, with the exception of two latitude bands in the central Pacific during PEM-Tropics A, the observed OH trends could be reasonably well understood in terms of measured precursor levels when used in conjunction with current photochemical mechanisms. The average agreement between box models and the OH observations for the central Pacific was a factor of 1.5. However, the box model results for all three central Pacific data sets tended to be higher than the observations for altitudes ≤5 km. For the two P-3B data sets this was also true for altitudes ≤ 8 km. For the DC-8 data, the model results above 5 km were systematically lower than the observations by an average factor of 1.4. Although one might be tempted to interpret these results as suggesting a systematic bias between models and observations, we believe at this time it would be premature to draw such a conclusion. In general, there was also good agreement between the box model results and those from the 3-D model, and hence, between the 3-D model and the observations.

When comparing the OH observations recorded on two different instruments (mounted on two different aircraft), the agreement, as defined in terms of the ratio of SICIMS to ATHOS, was relatively good, ranging between 1.3 to 0.6. However, because of the high level of correspondence in precursor profiles measured on the two aircraft, the trends in the two OH data sets would seem to suggest a possible altitude bias in one or both instruments. The results showed that the SICIMS instrument typically measured higher values at altitudes below 2 km and the ATHOS instrument measured higher values above 4 km. Clearly, more rigorous OH intercomparison work should be explored in future campaigns.

The general overall level of correspondence between the model results and observations suggests that for relatively clean background air, as defined by the central Pacific Basin, current OH model mechanisms do a reasonably good job. And because of the similarities in the chemical mechanisms employed in 3-D models, it could be further argued that a higher level of confidence is justified in tropical 3-D OH predictions. However, there continues to be a need to test and compare models with observations over a much broader range of environments, e.g., those at mid and high latitudes and those involving highly elevated levels of reactive hydrocarbons.

Acknowledgments. The author D. Davis would like to acknowledge the partial support of this research by NASA grant NCC-1-306. He would also like to thank the many students that helped in developing several of the plates in this paper, as well as the NASA pilots and flight crews who collectively made the collection of this massive data set possible.

References

Atkinson, R., D. L. Baulch, R. A. Cox, R. F. Hampson Jr., J. A. Kerr, and J. Troe, Evaluated kinetic and photochemical data for atmospheric chemistry, Supplement IV, IUPAC subcommittee on gas kinetic data evaluation for atmospheric chemistry, *J. Phys. Chem. Ref. Data, 21,* 1125-1568, 1992.

Ayers, G. P., S. A. Penkett, R. W. Gillett, B. Bandy, I. E. Galbally, C. M. Meyer, M. Elsworth, S. T. Bentley, and B. W. Forgan, Photochemical production of hydrogen peroxides and destruction of ozone in marine air over the southern ocean, *Nature, 360,* 446-449, 1992.

Ayers, G. P., S. A. Penkett, R. W. Gillett, B. J. Bandy, I. E. Galbally, C. P. Meyer, M. Elsworth, S. T. Bentley, and B. W. Forgan, Annual cycle of peroxides and ozone in marine air at Cape Grim, Tasmania, *J. Atmos. Chem., 23,* 221-252, 1996.

Benkovitz, C.M., T. Scholtz, J. Pacyna, L. Tarrassn, J. Dignon, E. Voldner, P.A. Spiro, J.A. Logan, and T.E. Graedel, Global inventories of anthropogenic emissions of SO_2 and NO_x, *J. Geophys. Res., 101,* 29,239-29,253, 1996.

Bradshaw, J., S. Sandholm, R. Talbot, H. Singh, G. Gregory, G. Sachse, and D. Blake, An Update on reactive odd-nitrogen measurements made during recent NASA Global Tropospheric Experiment Program, *J. Geophys. Res., 103,* 19,129-19,148, 1998.

Brune, W. H., et al., Airborne in situ OH and HO_2 observations in the cloud-free troposphere and stratosphere during SUCCESS, *Geophys. Res Lett , 25,* 1701-1704, 1998.

Brune, W. H., et al., OH and HO_2 chemistry in the North Atlantic free troposphere, *Geophys. Res. Lett., 26,* 3077-3080, 1999.

Chameides, W. L., and A. Tan, The two-dimensional diagnostic model for tropospheric OH: An uncertainty analysis, *J. Geophys. Res., 86,* 5209-5223, 1981.

Chameides, et al., Observed and model-calculated NO_2/NO ratios in tropospheric air sampled during the NASA GTE/CITE 2 field study, *J. Geophys. Res., 95,* 10,235-10,247, 1990.

Chen, G., A study of tropospheric photochemistry in the subtropical/tropical North and South Atlantic, Ph.D. thesis, GA Inst. of Tech., Atlanta, 1995.

Chen, G., et. al., An assessment of HO_x chemistry in the tropical Pacific boundary layer: Comparison of observations with model simulations during PEM Tropics A, *J. Atmos. Chem.*, 38, 317-344, 2001.

Crawford, J., et al., Photostationary state analysis of the NO_2-NO system based on airborne observations from the western and central North Pacific, *J. Geophys. Res., 101,* 2053-2072, 1996.

Crawford, J., et al., Implications of large scale shifts in tropospheric NO_x levels in the remote tropical Pacific, *J Geophys. Res., 102,* 28,447-28,468, 1997a.

Crawford, J., et al., An assessment of ozone photochemistry in the extratropical western North Pacific: Impact of continental outflow during the late winter/earlier spring, *J. Geophys. Res., 102,* 28,469-28,487, 1997b.

Crawford, J., et al., Assessment of upper tropospheric HO_x sources over the tropical Pacific based on NASA GTE/PEM data: Net effect on HO_x and other photochemical parameters, *J. Geophys. Res., 104,* 16,255-16,273, 1999a.

Crawford, J., D. Davis, G. Chen, R. Shetter, M. Müller, J. Barrick, and J. Olson, An assessment of cloud effects on photolysis rate coefficients: Comparison of experimental and theoretical values, *J. Geophys. Res., 104,* 5725-5734, 1999b.

Davis, D. D., et al., Photostationary state analysis of the NO_2-NO system based on airborne observations from the subtropical/tropical North and South Atlantic, *J. Geophys. Res., 98,* 23,501-23,523, 1993.

Davis, D. D., et al., Assessment of the ozone photochemistry tendency in the western North Pacific as inferred from PEM-West A observations during the fall of 1991, *J. Geophys. Res., 101,* 2111-2134, 1996.

DeMore, W. B., S. P. Sander, D. M. Golden, R. F. Hampson, M. J. Kurylo, C. J. Howard, A. R. Ravishankara, C. E. Kolb, and M. J. Molina, Chemical kinetics and photochemical data for use in stratospheric modeling, *JPL Publ., 97-4,* 1997.

Eisele, F. L., and D. J. Tanner, Ion assisted tropospheric OH measurement, *J. Geophys. Res., 96,* 9295-9308, 1991.

Eisele, F. L., and D. J. Tanner, Measurement of the gas phase concentration of H_2SO_4 and methane sulfonic acid and estimates of H_2SO_4 production and loss in the atmosphere, *J. Geophys. Res., 98,* 9001-9010, 1993.

Eisele, F. L., D. J. Tanner, C. A., Cantrell, and J. G. Calvert, Measurements and steady state calculations of OH concentrations at Mauna Loa observatory, *J Geophys Res.,101,* 14,665- 14,679, 1996.

Eisele, F. L., et al., The relationship between P-3B and DC-8 OH measurements during PEM-Tropics B, *J. Geophys. Res.*, this issue.

Fan, S.-M., D. J. Jacob, D. L. Mauzerall, J. D. Bradshaw, S. T. Sandholm, D. R. Blake, H. B. Singh, R. W. Talbot, G. L. Gregory, and G. W. Sachse, Origin of tropospheric NO_x over subarctic eastern Canada in summer, *J. Geophys. Res., 99,* 16,867-16,877, 1994.

Fuelberg, H. E., R. E. Newell, S. P. Longmore, Y. Zhu, D. J. Westberg, E. V. Browell, D. R. Blake, G. L. Gregory, and G. W. Sachse, A meteorological overview of the Pacific Exploratory Mission (PEM) Tropics period, *J. Geophys. Res., 104,* 5585-5622, 1999.

Fuelberg, H.E., R.E. Newell, D.J. Westberg, J.C. Maloney, J.R. Hannan, B.D. Martin, M.A. Avery, and Y. Zhu, A meteorological overview of the second Pacific Exploratory Mission in the tropics, *J. Geophys. Res.*, this issue.

Guenther, A., et al., A global model of natural volatile organic compound emissions, *J. Geophys. Res., 100,* 8873-8892, 1995.

Hansen, J., G. Russel, D. Rind, P. Stone, A. Lacis, S. Lebedeff, R. Ruedy, and L. Travis, Efficient three-dimensional global models for climate studies: Models I and II, *Mon. Weather Rev., 111,* 609-662, 1983.

Harder, J. W., R. O. Jakoubek, and G. H. Mount, Measurement of tropospheric trace gases by long-path differential absorption spectroscopy during the 1993 OH Photochemistry Experiment, *J. Geophys. Res., 102,* 6215-6226, 1997.

Hauglustaine, D. A., S. Madronich, B. Ridley, S. Flocks, C. Cantrell, F. Eisele, R. Shetter, D. Tanner, P. Ginoux, and E. Atlas, Photochemistry and budget of ozone during the Mauna Loa Observatory Photochemistry Experiment (MLOPEX 2), *J. Geophys. Res., 104,* 30,275-30,307, 1999.

Heikes, B. G., Formaldehyde and hydroperoxides at Mauna Loa Observatory, *J. Geophys. Res., 97,* 18,001-18,013, 1992.

Heikes, B. G., et al., Hydrogen peroxide and methylhydroperoxide distributions related to ozone and odd hydrogen over the North Pacific in the fall of 1991, *J. Geophys. Res., 101,* 1891-1905, 1996a.

Heikes, B. G., M. Lee, D. Jacob, R. Talbot, J. Bradshaw, H. Singh, D. Blake, B. Anderson, H. Fuelberg, and A. M. Thompson, Ozone hydroperoxides oxides of nitrogen, and hydrocarbon budgets in the marine boundary layer over the South Atlantic, *J. Geophys. Res., 101,* 24,221-24,235, 1996b.

Hoell, J. M., Jr., D. D. Davis, D. J. Jacob, M. O. Rogers, R. E. Newell, H. E. Fuelberg, R. J. McNeal, J. L. Raper, and R. J. Bendura, Pacific Exploratory Mission in the tropical Pacific: PEM-Tropics A, August-September, 1996, *J Geophys. Res , 104,* 5567-5583, 1999.

Hough, A. M., Development of a two-dimensional global tropospheric model: Model chemistry, *J. Geophys. Res., 96,* 7325-7362, 1991.

Jaeglé, L., D. J. Jacob, W. H. Brune, D. Tan, I. C. Faloona, A. J. Weinheimer, B. A. Ridley, T. L. Campos, and G. W. Sachse, Sources of HO_x and production of ozone in the upper troposphere over the United States, *Geophys. Res. Lett., 25,* 1709-1712, 1998.

Jaeglé, L., et. al., Ozone production in the upper troposphere and the influence of aircraft during SONEX: Approach of NOx-saturated conditions, *Geophys. Res. Lett , 26,* 3081-3084, 1999.

Jefferson, A., D. J. Tanner, F. L. Eisele, D. D. Davis, G. Chen, J. Crawford, J. W. Huey, A. L. Torres, and H. Berresheim, OH photochemistry and methane sulfonic acid formation in the coastal Antarctic boundary layer, *J. Geophys. Res , 103,* 1647-1656, 1998.

Lefer, B. L., S. R. Hall, L. Cinquini, J. D. Barrick, J. H. Crawford, and R. E. Shetter, NO_2 photolysis frequency measurements by scanning spectroradiometry during PEM-Tropics B: Comparison to filter radiometer measurements, *J. Geophys. Res* , this issue.

Levy, H., Normal atmosphere: Large radical and formaldehyde concentrations predicted, *Science, 173,* 141-143, 1971.

Levy, H., Photochemistry of the lower troposphere, *Planet. Space Sci., 20,* 919-935, 1972.

Logan, J. A., M. J. Prather, S. C. Wofsy, and M. B. McElroy, Tropospheric chemistry: A global perspective, *J. Geophys. Res., 86,* 7210-7254, 1981.

Lurmann, F. W., A. C. Lloyd, and R. Atkinson, A chemical mechanism for use in long-range transport/acid deposition computer modeling, *J. Geophys. Res., 91,* 10,905-10,936, 1986.

Mauldin, R. L. III, G. J. Frost, G. Chen, D. J. Tanner, A. S. H. Prevot, D. D. Davis, and F. L. Eisele, OH Measurements during the First Aerosol Characterization Experiment (ACE 1): Observations and model comparisons, *J Geophys Res., 103,* 16,713-16,729, 1998.

Mauldin, R.L. III, et al., Measurements of OH aboard the NASA P-3 during PEM-Tropics B, *J Geophys Res* , this issue.

McKeen, S. A., et al., Photochemical modeling of hydroxyl and its relationship to other species during the Tropospheric OH Photochemistry Experiment, *J Geophys. Res., 102,* 6467-6493, 1997.

Mount, G. H., The measurement of tropospheric OH by long path absorption, 1, Instrumentation, *J. Geophys. Res., 97,* 2427-2444, 1992.

Olson, J. R., B. A. Baum, D. R. Cahoon, and J. H. Crawford, Frequency and distribution of forest, savanna, and crop fires over tropical regions during PEM-Tropics A, *J. Geophys. Res., 104,* 5865-5876, 1999.

Olson, J. R., et al., Seasonal differences in the photochemistry of the South Pacific: A comparison of observations and model results form PEM-Tropics A and B, *J. Geophys. Res* , this issue.

Penkett, S. A., C. E. Reeves, B. J. Bandy, J. M. Kent, and H. R. Richer, Comparison of calculated and measured peroxide data collected in marine air to investigate prominent features of the annual cycle of ozone in the troposphere, *J. Geophys. Res., 103,* 13,377-13,388, 1998.

Price, C., and D. Rind, Modeling global lightning distributions in a general circulation model, *Mon. Weather Rev., 122,* 1930-1939, 1994.

Raper, J. L., M. M. Kleb, D. J. Jacob, D. D. Davis, R. E. Newell, H. E., Fuelberg, R. J. Bendura, J. M. Hoell, and R. J. McNeal, Pacific Exploratory Mission in the Tropical Pacific: PEM-Tropics B, March-April 1999, *J. Geophys. Res* , this issue.

Ravetta, F., et al., Experimental evidence for the importance of cenvected methylhydroperoxide as a source of hydrogen oxide (HO_x) radicals in the tropical upper tropopause, *J.Geophys. Res.*, this issue.

Schultz, M., R. Schmitt, K. Thomas, and A. Volz-Thomas, Photochemical box modeling of long-range transport from North America to Tenerife during the North Atlantic Regional Experiment (NARE) 1993, *J. Geophys. Res., 103,* 13,477-13,488, 1998.

Spivakovsky, C. M., R. Yevich, J. A. Logan, S. C. Wofsy, M. B. McElroy, and M. J. Prather, Tropospheric OH in a three-dimensional chemical tracer model: An assessment based on observations of CH_3CCl_3, *J. Geophys. Res., 95,* 18,441-18,471, 1990.

Stamnes, K., S. C. Tsay, W. Wiscombe, and K. Jayaweera, Numerically stable algorithm for discrete-ordinate-method radiative transfer in multiple scattering and emitting layered media, *Appl Opt.*, 27, 2501-2509, 1988.

Talukdar, R. K., C. A. Longfellow, M. K. Gilles, and A. R. Ravishankara, Quantum yields of $O(^1D)$ in the photolysis of ozone between 289 and 329 nm as a function of temperature, *Geophys. Res. Lett., 25,* 143-146, 1998.

Tan, D., et al., OH and HO_2 in the tropical Pacific: Results from PEM-Tropics B, *J. Geophys. Res.*, this issue.

Tanner, D. J., and F. L. Eisele, Present OH measurement limits and associated uncertainties, *J. Geophys. Res., 100,* 2883-2892, 1995 .

Trainer, M. E., Y. Hsie, S. A. McKeen, R. Tallamraju, D. D. Parrish, F. C. Fehsenfeld, and S. C. Liu, Impact of natural hydrocarbons in hydroxyl and peroxy radicals at a remote site, *J. Geophys. Res., 92,* 11,879-11,894, 1987.

Wang, Y. H., and D. J. Jacob, Anthropogenic forcing on tropospheric ozone and OH since preindustrial times, *J. Geophys. Res., 103,* 31,123-31,135, 1998.

Wang, Y., D. J. Jacob, and J. A. Logan, Global simulation of tropospheric O_3-NO_x-hydrocarbon chemistry, 1, Model formulation, *J. Geophys. Res., 103,* 10,713-10,726, 1998a.

Wang, Y., J. A. Logan, and D. J. Jacob, Global simulation of tropospheric O_3-NO_x-hydrocarbon chemistry, 2, Model evaluation and global ozone budget, *J. Geophys. Res., 103,* 10,727-10,756, 1998b.

Wang, Y., et al., Factors controlling tropospheric O_3, OH, NO_X, and SO_2 over the tropical Pacific during PEM-Tropics B, *J. Geophys. Res.*, this issue.

Wennberg, P. O., et al., Removal of stratospheric O_3 by radicals - In-situ measurements of OH, HO_2, NO, NO_2, CLO, and BRO, *Science, 266,* 398-404, 1994.

Wennberg, P. O, T. F. Hanisco, R. C. Cohen, R. M. Stimpfle, L. B. Lapson, and J. G. Anderson, In-situ measurements of OH and HO_2 in the upper troposphere and stratosphere, *J. Atmos. Chem., 52,* 3413-3420, 1995.

Wennberg, P. O., et al., Hydrogen radicals, nitrogen radicals, and the production of O_3 in the upper troposphere, *Science, 279,* 49-53, 1998.

Wesely, M.L., Parameterization of surface resistance to gaseous dry deposition in regional-scale numerical models, *Atmos Environ., 23,* 1293-1304, 1989.

Yienger, J. J., and H. Levy II, Empirical model of global soil-biogenic NO_x emissions, *J. Geophys. Res , 100,* 11,447-11,464, 1995.

B. Anderson, M. Avery, J. Crawford, G. Sachse, and S. Vay, NASA Langley Research Center, Hampton, VA 23681, USA.

D. Blake and N. Blake, Department of Chemistry, University of California, Irvine, CA 92717, USA.

W. Brune, I. Faloona, and D. Tan, Department of Meteorology, Pennsylvania State University, University Park, PA 16802, USA.

C. Cantrell, F. Grahek, B. Lefer, L. Mauldin, D. Montzka, B. Ridley, R. Shetter, and J. Walega, National Center for Atmospheric Research, Boulder, CO 80307, USA.

M. Carroll, Department of Atmospheric, Oceanic, and Space Sciences, University of Michigan, Ann Arbor, MI 48109, USA.

G. Chen, D. Davis, F. Eisele, G. Grodzinsky, S. Sandholm, D. Tanner, and Y. Wang, School of Earth and Atmospheric Sciences, Georgia Institute of Technology, Atlanta, GA 30332-0340, USA. (douglas.davis@eas.gatech.edu)

B. Heikes and J. Snow, Graduate School of Oceanography, University of Rhode Island, Narragansett, RI 02882, USA.

D. O'Sullivan, Department of Chemistry, United States Naval Academy, Annapolis, MD 21402, USA.

(Received October 13, 2000; revised February 9, 2001;
accepted February 15, 2001)